Design and performance of broadly tunable, narrow line-width, high repetition rate 1310nm VCSELs for swept source optical coherence tomography

V. Jayaraman*[a], J. Jiang[b], B. Potsaid[b], G. Cole[c], J. Fujimoto[d], and A. Cable[b]
[a]Praevium Research, Inc. 5266 Hollister Avenue, Suite 224 Santa Barbara, CA 93111
[b]Thorlabs, 435 Route 206 North, Newton, NJ 07860
[c]Advanced Optical Microsystems 1243 W. El Camino Real Mountain View, CA 94040
[d]Massachusetts Institute of Technology 77 Massachusetts Avenue, Cambridge, MA 02139

ABSTRACT

MEMS tunable vertical cavity surface emitting laser (MEMS-VCSEL) development, over the past two decades, has primarily focused on communications and spectroscopic applications. Because of the narrow line-width, single-mode operation, monolithic fabrication, and high-speed capability of these devices, MEMS-VCSELs also present an attractive optical source for emerging swept source optical coherence tomography (SSOCT) systems. In this paper, we describe the design and performance of broadly tunable MEMS-VCSELs targeted for SSOCT, emphasizing 1310nm operation for cancer and vascular imaging. We describe the VCSEL structure and fabrication, employing a fully oxidized GaAs/AlxOy mirrors in conjunction with dielectric mirrors and InP-based multi-quantum well active regions. We also describe the optimization of MEMs speed and frequency response for SSOCT. Key results include 1310 nm VCSELs with >120nm dynamic tuning range and imaging rates near 1MHz, representing the widest VCSEL tuning range and some of the fastest swept source imaging rates thus far obtained. We also describe how low-noise semiconductor optical amplification boosts average optical power to the required levels, while maintaining superior OCT imaging quality and state of the art system sensitivity. Finally, we present measured multi-centimeter dynamic coherence length, and discuss the implications of VCSELs for OCT.

Keywords: VCSEL, Optical Coherence Tomography, Tunable Laser, Swept Source

1. INTRODUCTION

Optical Coherence Tomography (OCT) is an emerging medical imaging technology that enables subsurface micrometer-scale, cross-sectional and 3D imaging *in situ* and in real-time[1-3]. OCT is analogous to ultrasound B-mode imaging, except imaging is performed by measuring the echo time delay and intensity of back-reflected or backscattered light, typically in the 750-1400nm range, rather than sound. Typical imaging depths are from ~1mm to >10mm, depending on the scattering level of imaged tissue, the imaging mode, and light source coherence length. OCT spatial resolutions are 10-100X better than magnetic resonant imaging (MRI), computed tomography (CT) and ultrasound. Emerging applications of OCT in medical imaging are vast, ranging from already commercialized ophthalmic and vascular applications, to ongoing clinical investigations in dentistry, dermatology, engineered tissue assessment, characterization of airway and lungs, imaging of the human colon and kidney, esophageal microscopy, assessment of cerebral blood flow, image-guided tumor resection surgery, optical biopsy, endoscopic 3-D cancer imaging, and ex-vivo cancer imaging, to name only a few representative examples.

OCT has progressed since its first generation using time-domain detection (TD-OCT)[1], to spectral / Fourier domain (SD-OCT)[4-6] and swept source / Fourier domain (SS-OCT)[5, 7, 8] configurations. In recent years, SS-OCT has demonstrated significant advantages compared to the other configurations, with respect to imaging speed, imaging range, system sensitivity, and imaging wavelength flexibility. For these reasons, many next generation commercial OCT systems in development are based on the SS-OCT configuration.

*vijay@praevium.com, phone: 805-448-4008

Vertical-Cavity Surface-Emitting Lasers XVI, edited by Chun Lei, Kent D. Choquette, Proc. of SPIE Vol. 8276, 82760D · © 2012 SPIE · CCC code: 0277-786X/12/$18 · doi: 10.1117/12.906920

Figure 1 illustrates the basic principle of SS-OCT. Light from a frequency-swept laser source is split to both a reference mirror and a sample of interest. Backscattered and reflected light from the sample is interfered with reflection from the reference mirror. The beat or difference frequency measured depends on the delay between paths and the sweep rate of the laser source. At a fixed sweep rate, different beat frequencies correspond to different delays, or reflections from different depths in the sample. Thus, by linearizing and Fourier transforming the interference signal, it is possible to obtain an axial (z-direction) profile of reflection magnitude vs. depth. In conjunction with x-y scanning, multiple axial scans can be used to create 2D and 3D comprehensive, volumetric data sets that can be used to construct arbitrary cross-sectional images, projections along arbitrary axes, or renderings similar to MRI or CT.

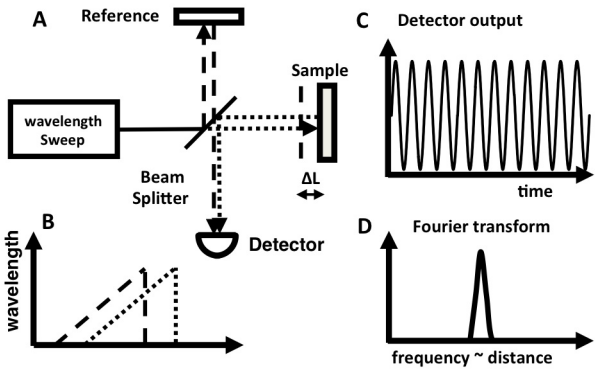

Figure 1: SSOCT system schematic, illustrating system elements (A), wavelength sweeps from reference (dashed in B) and sampled (dotted in B), detector output (C) and Fourier transform of detector output (D).

The wavelength (frequency) swept laser source shown in Fig. 1 is the critical enabling technology for SS-OCT. This fact has spurred a number of development efforts, employing varying approaches, aimed at creating the ideal SS-OCT tunable laser source. The desired performance parameters of a such a source include high maximum sweep rate, variable sweep rate, long dynamic source coherence length (equivalent to narrow dynamic line-width), and wide tuning range. High sweep rate is needed for real-time acquisition of large volumetric data sets[9], for reduced sensitivity to patient motion artifacts, and for imaging dynamically varying physiological processes. Variable sweep rates are highly desirable, as imaging range can be traded off with imaging speed, enabling different imaging modes in one application and with one instrument. Long coherence length is necessary for applications which require a long imaging range such as intravascular imaging, imaging the anterior eye, anatomic OCT, as well as non-destructive evaluation of larger objects. Wide sweep range is also critical, because the axial spatial resolution is inversely proportional to the laser sweep range[5].

A number of swept source laser configurations have been investigated in recent years. Three leading candidates include commercial short-cavity external cavity lasers (ECTL)[10], Fourier Domain Mode-Locked (FDML)[11] lasers, and vernier-tuning distributed bragg reflector (VT-DBR) lasers[12]. The ECTL configuration has been implemented in commercial devices with ~100nm tuning and variable axial scan rates up to 100kHz. FDML lasers have demonstrated 160nm tuning and ~350 kHz fundamental axial line rates which were multiplexed up to 1.4MHz using optical fiber delay lines[13]. Both the ECTL and FDML are multimode devices, which limits dynamic coherence length and imaging range to several mm. The ECTL tuning speed is limited by the round-trip time in an external laser cavity. The FDML circumvents this limitation by using a long fiber-optic external cavity, which has a round-trip time matched to the repetition rate of an intra-cavity filter. The sweep rate of the FDML, however, is fixed for a fixed fiber length. The FDML approach is also limited to wavelengths where low-loss optical fiber is available. The VT-DBR leverages WDM telecom tunable lasers originally developed for 1550nm operation in C and L bands. Its advantages include demonstrated commercial success for telecom, single-mode operation enabling long coherence length, pure electronic tuning without moving parts, enabling potentially very high sweep rates, and flexibility of scan rate and waveform. Recent commercial announcements indicate a tuning range of 100nm near 1310nm, and sweep rates up to 200kHz. Potential disadvantages of the VT-DBR include complexity of control, requiring mode hops to span tuning range, and a dependence on complex photonic integrated circuit technology, which may be difficult to transition to GaAs-based wavelengths.

The rest of this paper describes how the MEMS-VCSEL approach addresses many of the limitations above, and uniquely satisfies the requirements of SS-OCT systems. Though these devices have existed for nearly 2 decades, focus on other applications, along with limited tuning range and output power have, prior to this work, precluded successful application of MEMS-VCSELs to OCT.

2. WIDELY TUNABLE 1310NM VCSEL DESIGN AND FABRICATION

MEMS tunable VCSELs were conceived in the 1990s[14], and despite an initial focus on telecommunications[15], have evolved primarily for narrow spectroscopic applications[16, 17]. A number of features of these devices make them ideally suited to SSOCT. The short micrometer-scale cavity provides wide single longitudinal mode spacing, enabling wide continuous tuning range, and rapid build-up time to lasing[18]. Additionally, the low mirror mass and high mechanical resonance frequency[19-21] of these devices enables high-speed operation. Line-widths on the order of 3MHz have been demonstrated in fixed wavelength VCSELs[22]. In MEMS tunable VCSELs, additional mechanically induced chirp contributions can increase this to several hundred MHz[23], but a 300MHz line-width still corresponds to >40cm coherence length at 1310nm, which is ~2 orders of magnitude larger than multi-mode SS-OCT sources. These properties suggest MEMS-VCSELs have the potential be an ideal swept source for OCT.

Prior to 2011, MEMS-VCSELs did not have sufficient tuning range or output power to be suitable for OCT systems. Required tuning ranges at 1310nm are on the order of 100nm or higher, to enable imaging resolution competitive with external cavity devices. Required output powers need to be 30-50mW for emerging vascular and cancer-imaging applications. Prior to mid 2011, the maximum reported tuning range of any MEMS-VCSEL was 65nm at 1550nm[15], equivalent to about 55nm at the 1310nm vascular and cancer-imaging wavelength, assuming tuning range scales with wavelength. This previous work[15] also demonstrated an impressive 14mW peak power in an optically pumped device, which still remains significantly short of the levels required for OCT. In the past year, our VCSEL work has demonstrated >110nm[24] at 1310nm using optical pumping, and others have obtained up to 102nm at 1550nm using an electrically pumped design[25]. Our approach has been to focus on broadening tuning range, and rely on semiconductor optical amplification to provide high power and signal integrity for OCT systems. The details and results of this approach are described below.

Our approach to wide tuning range comprises at least 4 elements: 1. Thin active regions to provide wide free-spectral range, 2. Broadband mirrors to maintain low mirror loss over a wide wavelength range, 3. Bandgap-engineered wideband high gain active regions, and 4. Optical pumping. Optical pumping generally enables wider tuning range than electrical pumping because of reduced intra-cavity losses through elimination of dopants, elimination of resistive heating, and thinner active regions due to elimination of current-spreading layers. The swept source market for OCT is significantly less cost-sensitive than telecom, so the optically pumped approach is in the short-term commercially viable, though our approach includes pursuing lower-cost electrically pumped devices in a parallel development effort.

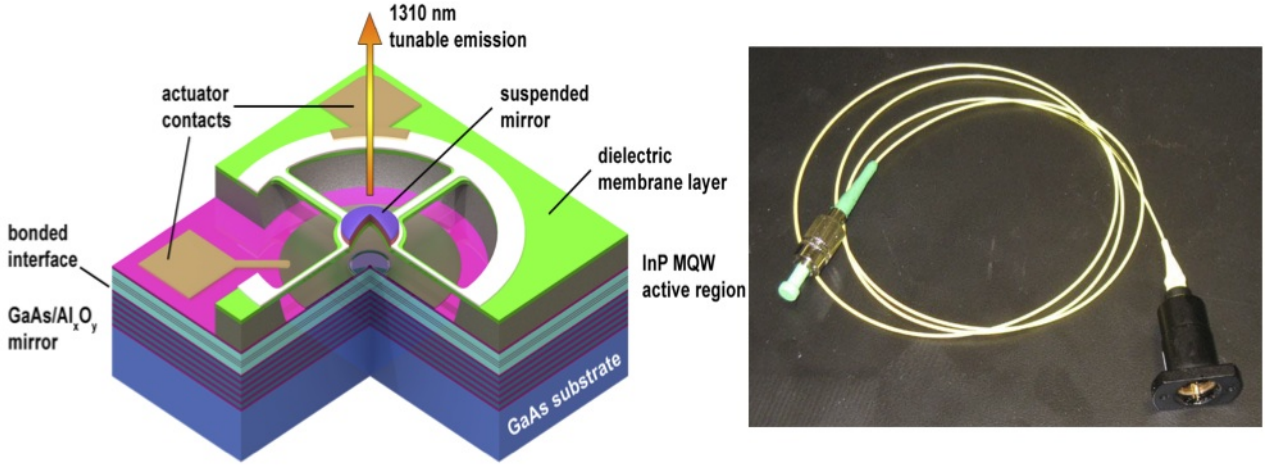

Figure 2: Three-dimensional VCSEL structure (left) and packaged VCSEL (right).

Figure 2 above illustrates a 3-dimensional cutaway view of the devices employed in this work. The structure uses a wide-gain bandgap-engineered InP-based multi-quantum well (MQW) active region joined by wafer bonding[26] to a wideband bottom GaAs-based fully oxidized AlxOy-GaAs mirror[27], and an integrated micromechanical actuator. In this configuration, the suspended top dielectric mirror is separated from the underlying "half-VCSEL" structure by an air-gap, which is tuned by electrostatic actuation. Two actuator contacts permit wire-bonding to the two electrodes of the MEMs structure. The VCSEL is optically pumped at 980nm through the top dielectric mirror, generating tunable 1310nm emission, which emerges from the top mirror and is amplified by a low-noise semiconductor optical amplifier (SOA), as shown below in Fig. 3. Though Fig. 2 shows 4 supporting struts, a variety of actuator designs with different numbers and dimensions of supporting struts, and different central plate diameters were fabricated for this work. Subsequent figures show representative results from a variety of devices. All data shown here were obtained with fiber-coupled devices using the package on the right of Fig. 2. This package is based on a transistor outline (TO) packaging platform developed in conjunction with our commercial partner Thorlabs. Figure 3 shows the main elements of the OCT testbed that is used to evaluate these devices for OCT imaging. Pump light is coupled into the fiber-coupled VCSEL through a 980/1310 WDM coupler, which separates the outgoing 1310nm radiation from the incoming 980nm pump light. After passing through an isolator, most of the1310nm light passes through a polarization controller, which aligns its polarization with a subsequent polarization-sensitive semiconductor optical amplifier. Amplified 1310nm emission is sent to the OCT imaging system. Prior to the OCT system, a portion of both post and pre-amplified 1310nm VCSEL emission is sent to a high-speed detector/oscilloscope and the optical spectrum analyzer (OSA) for device evaluation. The details of the OCT system are described elsewhere[9], and also at other presentations at this conference. The MEMS-VCSEL is driven by the amplified output of an arbitrary waveform generator.

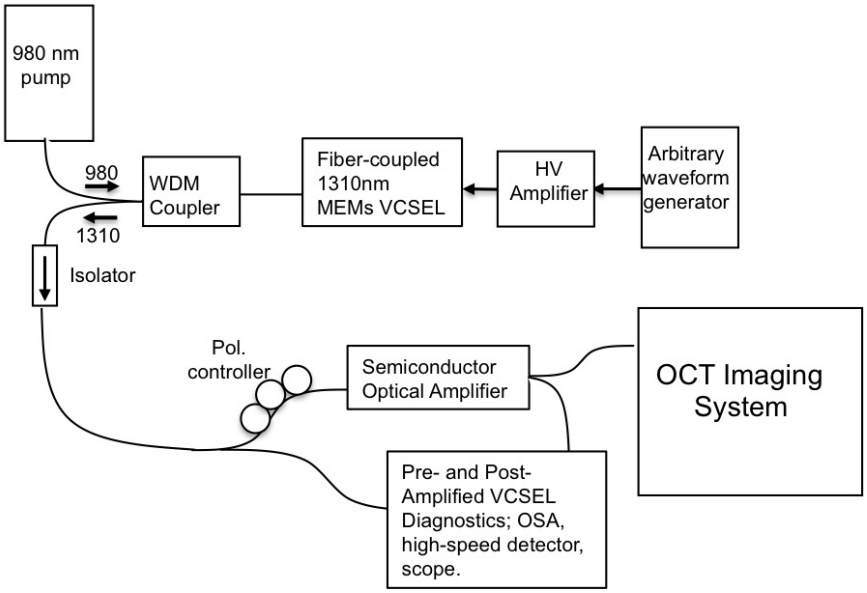

Figure 3: OCT system testbed for MEMS-Tunable VCSELs.

Figure 4 below illustrates the top and bottom mirror reflectivities associated with the device of Fig. 2. The top dielectric mirror has a bandwidth between first nulls of nearly 400nm. The bottom wafer-bonded fully oxidized mirror has a 700nm bandwidth between first nulls. We can define a "usable" bandwidth of each mirror as that range over which the mirror exceeds 99.6% reflectivity, roughly that value which is required for robust lasing in long-wavelength VCSELs. This bandwidth is ~200nm for the dielectric mirror and about ~500nm for the fully oxidized mirror. The combination of these two bandwidths is a critical contributor to obtaining the wide tuning ranges reported here. Also critical to obtaining this and wider tuning ranges is a wide-band high-gain multi-quantum well active region.

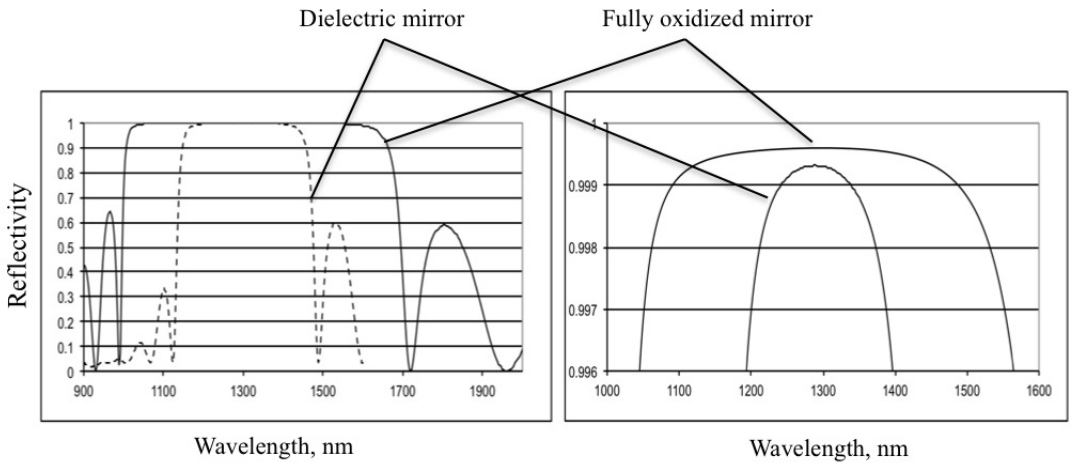

Figure 4: Mirror reflectivities of top (dielectric) and bottom(fully oxidized) mirrors of VCSEL.

3. STATIC AND DYNAMIC TUNING PERFORMANCE

Figures 5 below illustrates the wavelength vs. voltage and optical spectra over ~90V drive for one device under static tuned operation. The 111nm tuning range shown represents the widest ever reported for any MEMS tunable VCSEL. For static operation, tuning range of these devices is limited by "snapdown" considerations, which limit the reduction of airgap to nominally 1/3 of its zero-voltage value[28]. Under the typical dynamic sweeping used in OCT, however, the 1/3 gap rule can be exceeded, and wider tuning ranges can be obtained up to the device free-spectral range. Figure 6A illustrates the time-averaged spectrum of a device with 123nm dynamic tuning range, from 1237 to 1360nm, while swept at 200kHz. The narrowly peaked curve is the spectrum with no voltage applied, at ~1360nm, while the broadened curve shows the time-averaged spectrum under sinusoidal sweeping at 200kHz. This tuning range represents essentially one full free spectral range (125nm), using mirror deflections that exceed the 1/3 gap rule for static operation.

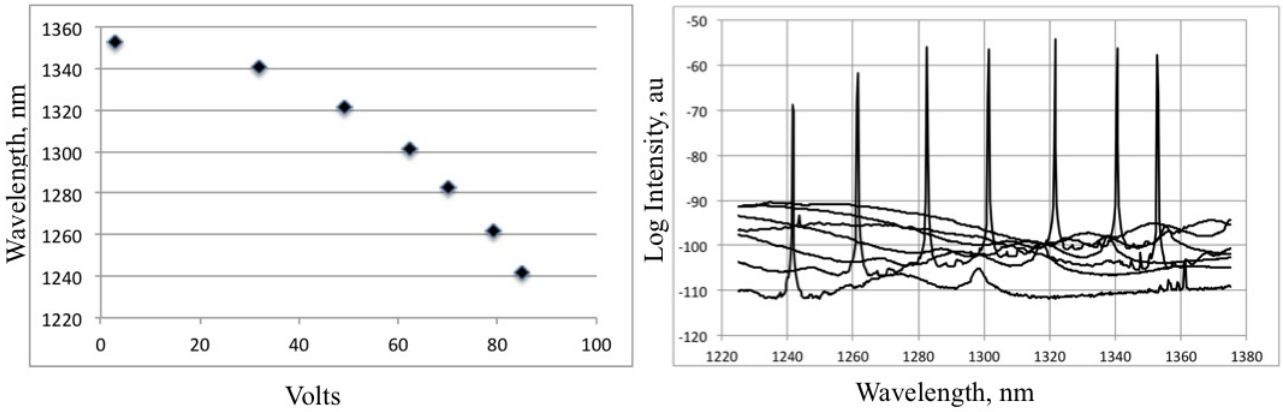

Figure 5: Representative Tuning Curve and spectra for ~111nm tuning from 1242-1353nm tuning.

We note the spectrum of Fig. 6A is non-uniform—showing >10dB drop in power from the 1360 nm long wavelength end to the 1237nm short-wavelength end. This non-uniformity can be linked to the non-uniformity in mirror reflectivity. The device of Figure 6A had its mirror reflectivity peaked near the short wavelength end of the tuning spectrum, so had larger output coupling at the long end of the spectrum, and power increase from short to longer wavelengths. Other devices with mirror peak position at different positions can show the opposite tuning slope, or nearly flat spectra. Figure 6B shows 3 different time averaged spectra with different mirror peak reflectivity positions, representing 3 generations of devices with ~100nm tuning and varying spectral shape. These curves illustrate the possibility of spectral shaping by judicious placement of the mirror peak reflectivity position.

The device results of Figs. 5 and 6 employ pump powers of ~10mW, and average fiber-coupled output powers of these devices under dynamic sweeping are typically several hundred microwatts. Use of a semiconductor optical amplifier boosts optical power to the ~30-50mW levels required for many OCT applications. Experiments with OCT system collaborators have demonstrated that the amplified VCSEL is sufficiently low noise to produce state of the art overall system sensitivity and superior OCT images. The amplifier can also advantageously shape the optical spectrum due to gain saturation. Figure 7 illustrates an example of post-amplified time-averaged spectrum. This spectrum can be further optimized by using, for example, the VCSEL spectrum of Figure 6B which is peaked near the edges, in conjunction with an amplifier peaked near the center of the tuning range, to increase the FWHM beyond that shown in Fig. 7.

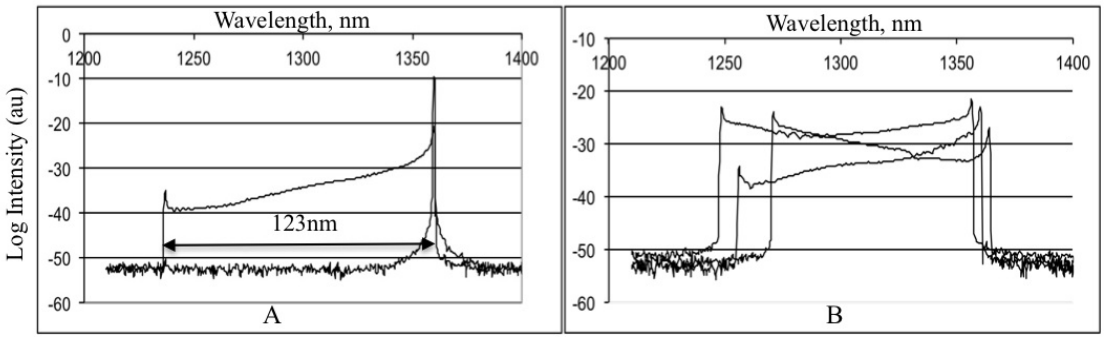

Figure 6: A.123nm dynamic tuning range. B. Various tuning slopes.

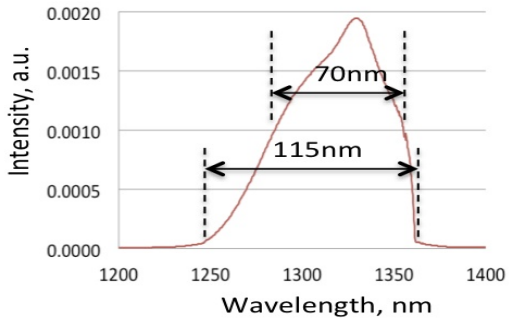

Figure 7: Post-amplified VCSEL spectrum under dynamic sweeping, linear scale. FWHM is 70 nm and full range is 115nm.

The tuning range results of Fig. 5-7, along with post amplified powers of 30-50mW represent the first MEMS-tunable VCSELs with static and dynamic performance adequate for emerging SSOCT systems. In the next section, we describe some unique OCT-related performance parameters provided by these devices.

4. OCT-RELEVANT PERFORMANCE PARAMETERS

The VCSELs described above, along with more recent 1050nm VCSELs, have been integrated into OCT test-beds at both Thorlabs and MIT. The details of this testbed, OCT system performance, and images obtained are described in more detail at in other papers at this conference. These papers describe record imaging speeds, record imaging range, variable imaging rates from 60kHz to 1.2Mhz, high quality leaf and human finger pad images, and imaging of the retina, anterior eye, and whole eye with a single swept source for the first time.

The purpose of this paper is to focus more closely on VCSEL performance parameters enabling the results above. In this section, we review 3 aspects of VCSEL performance relevant to OCT imaging. These are: 1. High wavelength sweep rate, 2. Variable sweep rates and linearized scanning, and 3. Long dynamic coherence length.

4.1 High wavelength sweep rate.

Figure 8 illustrates the wavelength tuning response of these VCSELs as a function of drive frequency applied to the MEMs actuator, for a variety of actuator geometries.

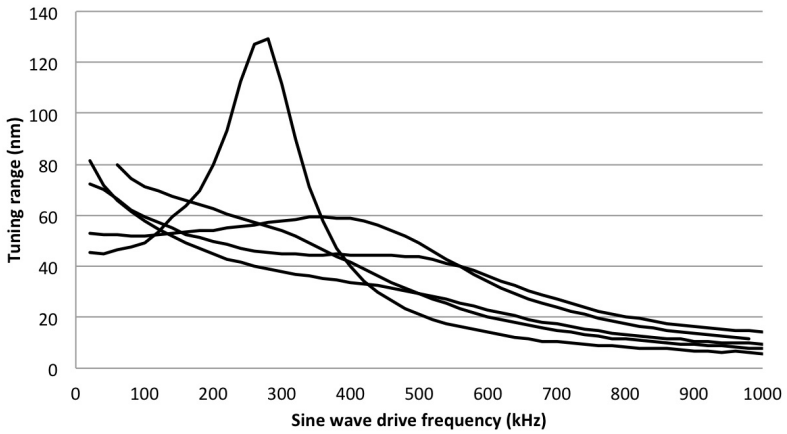

Figure 8: Sampling of frequency responses obtained by changing actuator geometry.

This figure illustrates that by varying the dimensions and number of supporting arms, as well as dimensions of central plate, it is possible to achieve a variety of resonant frequencies and damping ratios. This response includes contributions not only from actuator geometry, but also from film stress and squeeze film damping. Properly engineering the frequency response can create devices with sweep rates variable over a wide range, or, if desired, devices optimized to operate at a single frequency. Devices with flat frequency response have not only variable rates, but can also produce linearized wavelength vs. time trajectories by engineered drive waveforms.

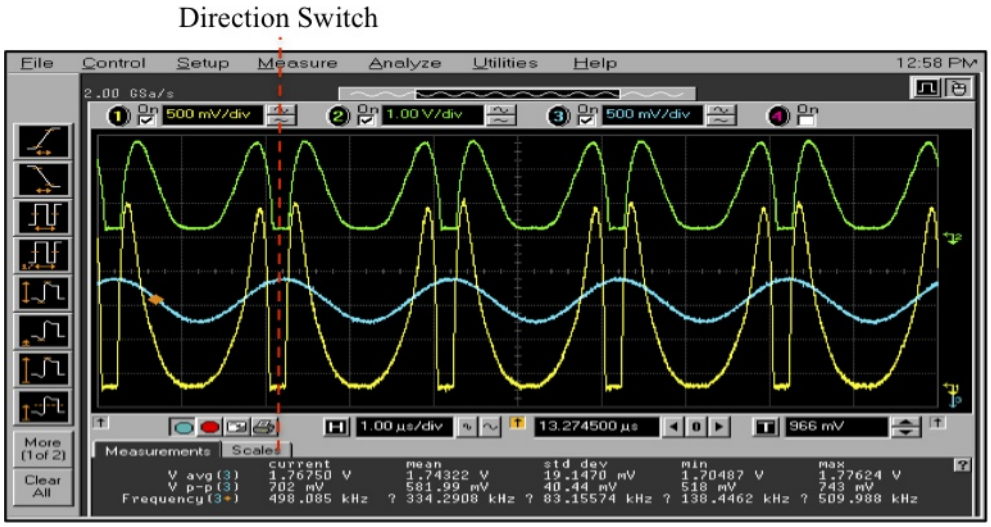

Figure 9: Oscilloscope Traces under 500kHz sinusoidal modulation, showing drive (blue), VCSEL power (green), and amplified VCSEL power (yellow). Powers are symmetric for forward and backward scans, enabling 1MHz bi-directional scanning.

Figure 9 above illustrates device response from one device driven with a 500kHz sine wave over ~100nm tuning range. The figure includes 3 oscilloscope traces including the drive waveform (blue curve), pre-amplified VCSEL power vs. time (green curve), and post-amplified VCSEL output power vs. time (yellow curve). The absence of power dropouts in the yellow curve indicates that the VCSEL is operating in a stable polarization state, since the amplifier used only amplifies one polarization. The absence of polarization switching is critical to obtaining high-quality OCT images. We also note that both yellow and green curves are symmetric with respect to the point at which sweep direction changes. This indicates that there is no laser degradation in one wavelength scan direction, in contrast to many previous swept sources. Use of both forward and backward wavelength scans enables an effective doubling of axial scan rate,

allowing 1MHz axial scan (A-scan) with a 500kHz drive waveform. This scan rate (more recently increased to 1.2MHz) represents the fastest axial scan rate ever achieved directly from a swept laser, with previous fastest obtained with FDML lasers[13].

4.2 Variable scan rate and linearized scanning

As discussed above, flat frequency response, like some of the curves shown in Fig. 8 above, enables variable rate linearized scanning from a single device. Figure 10 below illustrates results obtained with a single device driven over a 115nm tuning range at scan rates from 50kHz to 1 Mhz. The top row of traces shows the drive waveform applied to the MEMS actuator, while the bottom row shows the wavelength response vs. time. Plots A,B, and C show linearized scanning for a 100kHz drive/100kHz unidirectional axial scan (A), 50kHz drive/100kHz bidirectional scan (B), and 100kHz drive/200kHz bi-directional scan (C). Plot D illustrates a sinusoidal drive at 500kHz in combination with a sinusoidal response, which can be used for 1MHz bidirectional scanning. The combination of Figs. 10A-D illustrate the variety of drive conditions achievable for a single device. These allow a commonly required tradeoff between imaging speed and imaging range to be achieved with a single device.

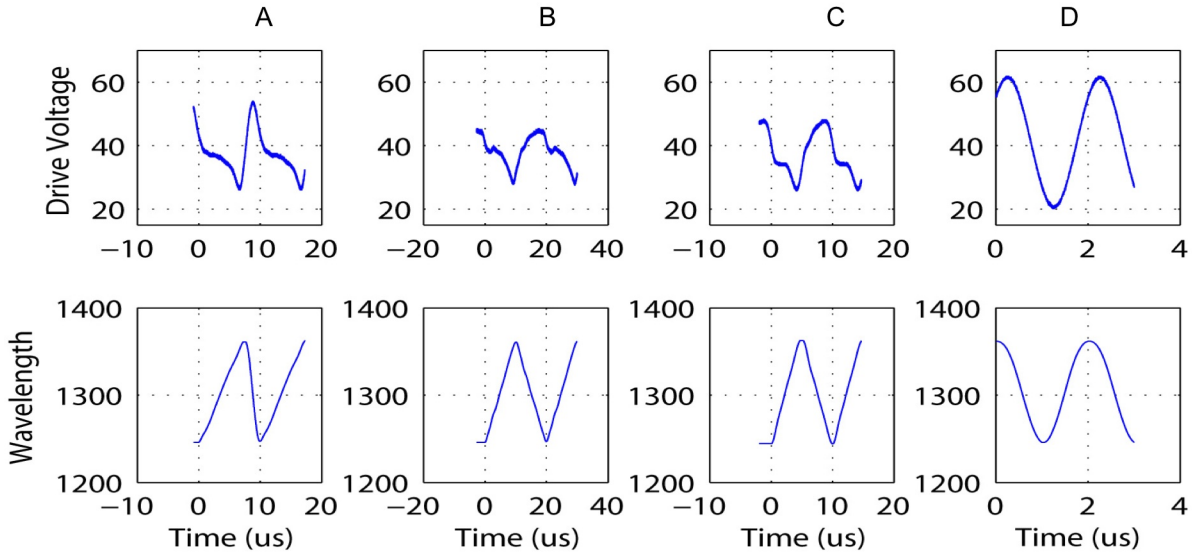

Figure 10: Variety of wavelength trajectories obtained by pre-shaping of drive waveform. These include A. 100kHz drive/100kHz unidirectional scan, B. 50kHz drive/100kHz bidirectional scan, C. 100kHz drive/200kHz bi-directional scan, and D. 500kHz drive/1MHz bi-directional scan.

4.3 Long dynamic coherence length

The static linewidths of MEMS tunable VCSELs have been measured in the range of a few hundred MHz. This corresponds to tens of cm coherence length. If this linewidth could be maintained under dynamic sweeping, it would exceed that required for virtually every biological application, where imaging depths vary from a few mm in highly scattering tissue, to up to several cm in lightly scattering ophthalmic applications. This suggests a fast swept VCSEL has broad applicability over a wide range of applications.

Under dynamic operation, coherence length in OCT systems is typically measured by evaluating the system sensitivity as a function of imaging depth, as shown in Fig. 11. The dynamic coherence length is defined as twice the imaging depth at which signal sensitivity drops by a factor of 2, since light traverses the imaging depth twice before being interfered with the reference beam. The measurement of dynamic coherence length is complicated by the need for increasingly high-speed detection electronics as sweep rate and coherence length is increased. Figure 11 shows a measurement using a swept VCSEL with a 60kHz unidirectional scan. As shown, negligible degradation of sensitivity is observed at 50mm imaging depth in air, corresponding to >>10cm coherence length. This dynamic performance is enabled by the absence of competing VCSEL modes, consistent with known static line-widths, and validates the VCSEL

as a swept source applicable to a variety of medical imaging applications. The measurement of Fig. 11 remains detection-limited, so the measured dynamic VCSEL coherence length is likely larger than measured.

5. CONCLUSIONS

The results presented here demonstrate that VCSELs provide unique advantages for OCT. The 1 MHz axial scan rate obtained by bidirectional frequency sweeping is the highest acquisition speed obtained directly from a swept laser. The sweep repetition rate does not appear to be limited by laser dynamics and higher speeds may be possible by changing MEMS mirror designs to support higher frequency drive. Higher speeds could also be obtained by multiplying the laser repetition rate using optical fiber delay lines as previously demonstrated with FDML swept lasers[13]. Ultrahigh sweep rate operation will be especially important for applications which require en face OCT image generation because each en face pixel requires an axial scan. The long imaging range is important for applications such as intravascular OCT which requires imaging the entire circumference of arteries irrespective of catheter centration, ophthalmic OCT of the anterior eye where imaging optical surfaces allows refractive power calculation, and anatomic OCT which involves profilometry of larger scale structures such as the upper airway. Long imaging range will also enable many applications in non-destructive evaluation, process control, and profilometry.

Further advantages of the VCSEL include wavelength flexibility, and migration to 1050nm VCSELs for retinal and anterior eye imaging[10] has recently been demonstrated, as described in other papers at this conference. Development of electrical[29] instead of optical pumping for VCSELs promises lower cost and miniaturization. Electrically pumped VCSELs have been demonstrated from wavelengths as short as 650nm[30] to as long as 2300nm[31], suggesting extension of VCSEL-based OCT to a wide variety of wavelengths.

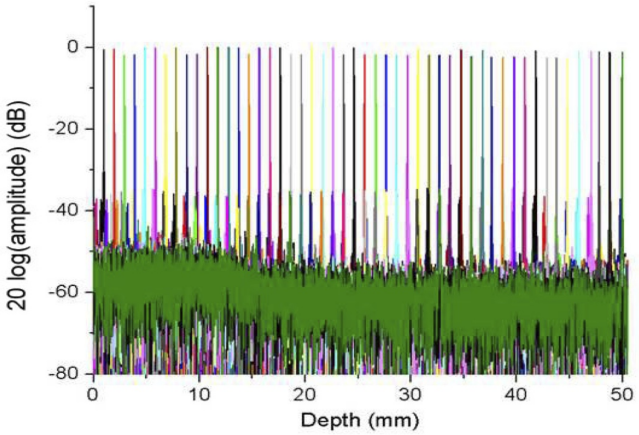

Figure 11: Normalized signal vs. imaging depth at 60kHz unidirectional scan. Dynamic coherence length is >>100mm.

ACKNOWLEDGEMENTS

This research was supported by NIH grant 2R44CA101067-05 and Thorlabs matching funds.

REFERENCES

[1] Huang, D., Swanson, E. A., Lin, C. P. *et al.*, "OPTICAL COHERENCE TOMOGRAPHY," Science, 254(5035), 1178-1181 (1991).

[2] Fujimoto, J. G., Pitris, C., Boppart, S. A. *et al.*, "Optical coherence tomography: An emerging technology for biomedical imaging and optical biopsy," Neoplasia, 2(1-2), 9-25 (2000).

[3] Fujimoto, J. G., "Optical coherence tomography for ultrahigh resolution in vivo imaging," Nature Biotechnology, 21(11), 1361-1367 (2003).

[4] Leitgeb, R., Hitzenberger, C. K., and Fercher, A. F., "Performance of fourier domain vs. time domain optical coherence tomography," Optics Express, 11(8), 889-894 (2003).

[5] Choma, M. A., Sarunic, M. V., Yang, C. H. *et al.*, "Sensitivity advantage of swept source and Fourier domain optical coherence tomography," Optics Express, 11(18), 2183-2189 (2003).

[6] Yun, S. H., Tearney, G. J., Bouma, B. E. *et al.*, "High-speed spectral-domain optical coherence tomography at 1.3 mu m wavelength," Optics Express, 11(26), 3598-3604 (2003).

[7] Chinn, S. R., Swanson, E. A., and Fujimoto, J. G., "Optical coherence tomography using a frequency-tunable optical source," Optics Letters, 22(5), 340-342 (1997).

[8] Yun, S. H., Tearney, G. J., de Boer, J. F. *et al.*, "High-speed optical frequency-domain imaging," Optics Express, 11(22), 2953-2963 (2003).

[9] Adler, D. C., Chen, Y., Huber, R. *et al.*, "Three-dimensional endomicroscopy using optical coherence tomography," Nature Photonics, 1(12), 709-716 (2007).

[10] Potsaid, B., Baumann, B., Huang, D. *et al.*, "Ultrahigh speed 1050nm swept source / Fourier domain OCT retinal and anterior segment imaging at 100,000 to 400,000 axial scans per second," Optics Express, 18(19), 20029-20048 (2010).

[11] Huber, R., Adler, D. C., and Fujimoto, J. G., "Buffered Fourier domain mode locking: unidirectional swept laser sources for optical coherence tomography imaging at 370,000 lines/s," Optics Letters, 31(20), 2975-2977 (2006).

[12] George, B., and Derickson, D., "High-Speed Concatenation of Frequency Ramps Using Sampled Grating Distributed Bragg Reflector Laser Diode Sources for OCT Resolution Enhancement," Proceedings of the SPIE - The International Society for Optical Engineering, 7554, (2010).

[13] Klein, T., Wieser, W., Eigenwillig, C. M. *et al.*, "Megahertz OCT for ultrawide-field retinal imaging with a 1050nm Fourier domain mode locked laser," Optics Express, 19(4), 3044-30623062 (2011).

[14] Wu, M. S., Vail, E. C., Li, G. S. *et al.*, "Tunable micromachined vertical cavity surface emitting laser," Electronics Letters, 31(19), 1671-16721672 (1995).

[15] Matsui, Y., Vakhshoori, D., Peidong, W. *et al.*, "Complete polarization mode control of long-wavelength tunable vertical-cavity surface-emitting lasers over 65-nm tuning, up to 14-mW output power," IEEE Journal of Quantum Electronics, 39(9), 1037-10481048 (2003).

[16] Lackner, M., Schwarzott, M., Winter, F. *et al.*, "CO and CO 2 spectroscopy using a 60 nm broadband tunable MEMS-VCSEL at ap1.55 mum," Optics Letters, 31(21), 3170-31723172 (2006).

[17] Svensson, T., Andersson, M., Rippe, L. *et al.*, "VCSEL-based oxygen spectroscopy for structural analysis of pharmaceutical solids," Applied Physics B: Lasers and Optics, 90(2), 345-354354 (2008).

[18] Huber, R., Wojtkowski, M., Taira, K. *et al.*, "Amplified, frequency swept lasers for frequency domain reflectometry and OCT imaging: design and scaling principles," Optics Express, 13(9), 3513-3528 (2005).

[19] Huang, M. C. Y., Zhou, Y., and Chang-Hasnain, C. J., "A nanoelectromechanical tunable laser," Nature Photonics, 2(3), 180-184 (2008).

[20] Cole, G. D., Bowers, J. E., Turner, K. L. *et al.*, "Dynamic characterization of MEMS-tunable vertical-cavity SOAs," IEEE/LEOS Optical MEMs 2005 (IEEE Cat. No. 05EX1115), 99-100100 (2005).

[21] Cole, G. D., Behymer, E., Bond, T. C. *et al.*, "Short-wavelength MEMS-tunable VCSELs," Optics Express, 16(20), 16093-16103 (2008).

[22] di Sopra, F. M., Zappe, H. P., Moser, M. *et al.*, "Near-infrared vertical-cavity surface-emitting lasers with 3-MHz linewidth," IEEE Photonics Technology Letters, 11(12), 1533-1535 (1999).

[23] Halbritter, H., Sydlo, C., Kogel, B. *et al.*, "Linewidth and chirp of MEMS-VCSELs," IEEE Photonics Technology Letters, 18(17-20), 2180-2182 (2006).

[24] Jayaraman, V., Jiang, J., Li, H. *et al.*, "OCT Imaging up to 760 kHz Axial Scan Rate Using Single-Mode 1310nm MEMS-Tunable VCSELs with >100nm Tuning Range," CLEO: 2011 - Laser Science to Photonic Applications, 2 pp.-2 pp.2 pp. (2011).

[25] Gierl, C., Gruendl, T., Debernardi, P. *et al.*, "Surface micromachined tunable 1.55 mu m-VCSEL with 102 nm continuous single-mode tuning," Optics Express, 19(18), 17336-17343 (2011).
[26] Jayaraman, V., Goodnough, T. J., Beam, T. L. *et al.*, "Continuous-wave operation of single-transverse-mode 1310-nm VCSELs up to 115 degrees C," IEEE Photonics Technology Letters, 12(12), 1595-1597 (2000).
[27] MacDougal, M. H., Dapkus, P. D., Bond, A. E. *et al.*, "Design and fabrication of VCSELs with Al xO y-GaAs DBRs," IEEE Journal of Selected Topics in Quantum Electronics, 3(3), 905-915915 (1997).
[28] Chang-Hasnain, C. J., "Tunable VCSEL," IEEE Journal of Selected Topics in Quantum Electronics, 6(6), 978-987 (2000).
[29] Jayaraman, V., Mehta, M., Jackson, A. W. *et al.*, "High-power 1320-nm wafer-bonded VCSELs with tunnel junctions," IEEE Photonics Technology Letters, 15(11), 1495-14971497 (2003).
[30] Knigge, A., Zorn, M., Weyers, M. *et al.*, "High-performance vertical-cavity surface-emitting lasers with emission wavelength between 650 and 670 nm," Electronics Letters, 38(16), 882-883 (2002).
[31] Boehm, G., Bachmann, A., Rosskopf, J. *et al.*, "Comparison of InP- and GaSb-based VCSELs emitting at 2.3 mu m suitable for carbon monoxide detection," Journal of Crystal Growth, 323(1), 442-445 (2011).